Inorg. Chem. **2002**, *41*, 4453–4460

Solid-State Structural and Magnetic Investigations of $\{M[HC(3,5\text{-}Me_2pz)_3]_2\}(BF_4)_2$ (M = Fe, Co, Ni, Cu): Observation of a Thermally Induced Solid-State Phase Change Controlling an Iron(II) Spin-State Crossover

Daniel L. Reger,* Christine A. Little, and Mark D. Smith

Department of Chemistry and Biochemistry, University of South Carolina, Columbia, South Carolina 29208

Gary J. Long

Department of Chemistry, University of Missouri—Rolla, Rolla, Missouri 65409-0010

Received December 11, 2001

The reaction of $M(BF_4)_2 \cdot xH_2O$ (M = Co, Ni, and Cu) and $HC(3,5\text{-}Me_2pz)_3$ in a 1:2 ratio yields $\{Co[HC(3,5\text{-}Me_2pz)_3]_2\}(BF_4)_2$ (**2**), $\{Ni[HC(3,5\text{-}Me_2pz)_3]_2\}(BF_4)_2$ (**3**), and $\{Cu[HC(3,5\text{-}Me_2pz)_3]_2\}(BF_4)_2$ (**4**). Over the temperature range from 5 to 350, 345, or 320 K, Curie law behavior is observed for microcrystalline samples of all three compounds showing them to have three, two, and one unpaired electrons, respectively, with no spin-crossover observed for **2**. Crystalline samples of these compounds torque in the applied magnetic field the first time the sample is cooled to 5 K. The solid-state structures of all three are isomorphous at 220 K, monoclinic in the space group *C*2/*c*. The metal is located on a unique crystallographic site and has a trigonally distorted octahedral structure, with **4** showing the expected Jahn–Teller distortions. Cooling crystals of all three to low temperatures leads to the observation of the same phase change to triclinic in the new space group $P\bar{1}$ with nonmerohedral twinning. This change is reversible and yields two crystallographically unique metal sites at low temperature. The bond angles and distances for the two different metal sites for each compound in the low temperature structures are very similar to each other and to those in the 220 K structures. The same phase change, monoclinic to triclinic, has been observed previously for $\{Fe[HC(3,5\text{-}Me_2pz)_3]_2\}(BF_4)_2$ (**1**), except in this case, the phase change results in half of the cations changing over from the high-spin state to the low-spin state while the other half of the cations remain high-spin, with the low-spin form decreasing its Fe–N bond distances by 0.19 Å. The new results with **2**–**4** show that it is the phase transition, which occurs in complexes of the type $\{M[HC(3,5\text{-}Me_2pz)_3]_2\}(BF_4)_2$ with first row transition metals, that is driving the unusual spin-crossover behavior of $\{Fe[HC(3,5\text{-}Me_2pz)_3]_2\}(BF_4)_2$.

Introduction

The properties of octahedral transition metal complexes, especially those with an FeN_6 central core, that undergo thermal spin conversions between the high-spin (HS, $S = 2$) and low-spin (LS, $S = 0$) states have been widely investigated.[1] In general, complexes which are HS in the solid state at room temperature may show a spin crossover to the LS electronic state upon cooling.[1,2] Iron(II) complexes provide the classic example of spin-crossover complexes; however, other metals including cobalt(II) have been shown to exhibit this behavior as well.[3]

We have prepared new iron(II) complexes of the tris(pyrazolyl)methane family of ligands[4] and have shown that these complexes have unusual spin-crossover properties. The most interesting results thus far have come from the complex $\{Fe[HC(3,5\text{-}Me_2pz)_3]_2\}(BF_4)_2$ (**1**). Even though only one iron

* To whom correspondence should be addressed. E-mail: reger@psc.sc.edu.

(1) (a) Gütlich, P. In *Mössbauer Spectroscopy Applied to Inorganic Chemistry*; Long, G. J., Ed.; Plenum: New York, 1984; Vol. 1, p 287. (b) Gütlich, P.; Hauser, A.; Spiering, H. *Angew. Chem., Int. Ed. Engl.* **1994**, *33*, 2024. (c) Kahn, O.; Martinez, J. *Science* **1998**, *279*, 44.

10.1021/ic0112645 CCC: $22.00
Published on Web 07/12/2002

site is observed by X-ray crystallography at ambient temperature, crystalline samples change abruptly from all HS above 206 K to a 50:50 mixture of HS and LS below 200 K, and the composition of this lower temperature mixture does not change as the temperature is lowered to 5 K.[4a] Clear, colorless crystals of $\{Fe[HC(3,5\text{-}Me_2pz)_3]_2\}(BF_4)_2$ cooled to 173 K are purple in color and the crystal system has changed from C-centered monoclinic to primitive triclinic. This change yields two crystallographically different iron(II) sites below 200 K where half of the iron(II) cations remain HS while the other half become LS, with reduced Fe−N bond distances of ca. 0.2 Å (the difference in bond length expected for HS versus LS iron(II) complexes).

We have now prepared analogous $\{M[HC(3,5\text{-}Me_2pz)_3]_2\}(BF_4)_2$ complexes with cobalt(II), nickel(II), and copper(II). Our initial goal was to determine if the cobalt(II) complex would show spin-crossover behavior.[3,5] As reported here, $\{Co[HC(3,5\text{-}Me_2pz)_3]_2\}(BF_4)_2$ does *not* undergo a spin change at low temperatures, but X-ray crystallography shows that the crystals undergo the identical phase change observed for crystals of $\{Fe[HC(3,5\text{-}Me_2pz)_3]_2\}(BF_4)_2$. These results caused us to expand the investigation to the nickel(II) and copper(II) complexes, complexes that we show here also undergo the identical phase change observed for $\{Fe[HC(3,5\text{-}Me_2pz)_3]_2\}(BF_4)_2$.

Experimental Section

General Procedures. All operations were carried out under a nitrogen atmosphere using either standard Schlenk techniques or in a Vacuum Atmospheres HE-493 drybox. All solvents were dried and distilled prior to use. Proton NMR chemical shifts are reported in ppm versus TMS. $Co(BF_4)_2\cdot 6H_2O$, $Ni(BF_4)_2\cdot 6H_2O$, and $Cu(BF_4)_2\cdot xH_2O$ were purchased from Aldrich chemicals. $HC(3,5\text{-}Me_2pz)_3$ was prepared according to our recently reported procedures.[6] Elemental analyses were performed by Robertson Microlit Laboratories, Inc.

(2) (a) Grandjean, F.; Long, G. J.; Hutchinson, B. B.; Ohlhausen, L.; Neill, P.; Holcomb, J. D. *Inorg. Chem.* **1989**, *28*, 4406. (b) Long, G. J.; Hutchinson, B. B. *Inorg. Chem.* **1987**, *26*, 608. (c) Jesson, J. P.; Trofimenko, S.; Eaton, D. R. *J. Am. Chem. Soc.* **1967**, *89*, 3158. (d) Jesson, J. P.; Weiher, J. F.; Trofimenko, S. *J. Chem. Phys.* **1968**, *48*, 2058. (e) Cartier dit Moulin, C.; Rudolf, P.; Flank, A.-M.; Chen, C.-T. *J. Phys. Chem.* **1992**, *96*, 6196. (f) Cartier dit Moulin, C.; Sainctavit, P.; Briois V. *Jpn. J. Appl. Phys.* **1993**, *32* (Suppl. 32-2), 38. (g) Briois, V.; Cartier dit Moulin, C.; Momenteau, M.; Maillard, P.; Zarembowitch, J.; Dartyge, E.; Fontaine, A.; Tourillon, G.; Thuéry, P.; Verdaguer, M. *J. Chim. Phys. Phys.-Chim. Biol.* **1989**, *86*, 1623. (h) Young, N. A. *J. Chem. Soc., Dalton Trans.* **1996**, 1275. (i) Real, J.-A.; Gallois, B.; Granier, T.; Suez-Panama, F.; Zarembowitch, J. *Inorg. Chem.* **1992**, *31*, 4972. (j) Real, J. A.; Castro, I.; Bousseksou, A.; Verdaguer, R. B.; Cartro, M.; Linares, J.; Varret, F. *Inorg. Chem.* **1997**, *36*, 455.

(3) Gaspar, A. B.; Muñoz, M. C.; Niel, V.; Real, J. A. *Inorg. Chem.* **2001**, *40*, 9 and references therein.

(4) (a) Reger, D. L.; Little, C. A.; Rheingold, A. L.; Lam, M.; Liable-Sands, L. M.; Rhagitan, B.; Concolino, T.; Mohan, A.; Long, G. J.; Briois, V.; Grandjean, F. *Inorg. Chem.* **2001**, *40*, 1508. (b) Reger, D. L.; Little, C. A.; Rheingold, A L.; Lam, K.-C.; Concolino, T.; Mohan, A.; Long, G. J. *Inorg. Chem.* **2000**, *39*, 4674. (c) Reger, D. L.; Little, C. A.; Rheingold, A L.; Sommer, R. D.; Long, G. J. *Inorg. Chim. Acta* **2001**, *316*, 65. (d) Reger, D. L.; Little, C. A.; Young, V. G.; Pink, M. *Inorg. Chem.* **2001**, *40*, 2870

(5) Hannay, C.; Hubin-Franskin, M.-J.; Grandjean, F.; Briois, V.; Itie, J.-P.; Polian, A.; Trofimenko, S.; Long, G. J. *Inorg. Chem.* **1997**, *32*, 55580.

(6) Reger, D. L.; Grattan, T. C.: Brown, K. J.; Little, C. A.; Lamba, J. J. S.; Rheingold, A L.; Sommer, R D. *J. Organomet. Chem.*, **2000**, *607*, 120.

Table 1. Crystallographic Data for the 220 K Structures of $\{Co[HC(3,5\text{-}Me_2pz)_3]_2\}(BF_4)_2$ (**2**), $\{Ni[HC(3,5\text{-}Me_2pz)_3]_2\}(BF_4)_2$ (**3**), and $\{Cu[HC(3,5\text{-}Me_2pz)_3]_2\}(BF_4)_2$ (**4**)

	2	**3**	**4**
formula	$CoN_{12}C_{32}H_{44}B_2F_8$	$NiN_{12}C_{32}H_{44}B_2F_8$	$CuN_{12}C_{32}H_{44}B_2F_8$
fw	829.34	829.12	833.95
space group	*C2/c*	*C2/c*	*C2/c*
cryst syst	monoclinic	monoclinic	monoclinic
a, Å	20.3012(12)	20.316(3)	20.3890(14)
b, Å	10.3039(6)	10.2919(15)	10.3782(7)
c, Å	19.6375(12)	19.622(3)	19.5811(14)
α, deg	90	90	90
β, deg	111.4640(10)	111.965(3)	112.6570(10)
γ, deg	90	90	90
V, Å^3	3822.9(4)	3804.9(10)	3823.6(5)
Z	4	4	4
ρ(calcd), g cm^{-3}	1.441	1.447	1.449
μ(Mo Kα), cm^{-1}	5.30	5.91	6.52
R1(*F*)[a], wR2(F^2)[a]	0.0437, 0.1036	0.0422, 0.0791	0.0423, 0.1224

[a] $R1 = \sum||F_o| - |F_c||/\sum|F_o|$. $wR2 = \{\sum[w(F_o^2 - F_c^2)^2]/\sum[w(F_o^2)^2]\}^{1/2}$; $w = 1/[\sigma^2(F_o^2) + (aP)^2 + bP]$, where P is $[2F_c^2 + \max(F_o^2, 0)]/3$.

Magnetic susceptibilities were measured in gelatin capsules at 0.5 T with a Quantum Design MPMS XL SQUID magnetometer. A diamagnetic correction of 420×10^{-6} emu/mol was used to correct all the measured molar magnetic susceptibilities. The very small diamagnetic contribution of the gelatin capsules had a negligible contribution to the overall magnetization and was neglected.

$\{Co[HC(3,5\text{-}Me_2pz)_3]_2\}(BF_4)_2$ (2). $Co(BF_4)_2\cdot 6H_2O$ (0.13 g, 0.38 mmol) was suspended in THF (10 mL) and treated dropwise by cannula transfer with a THF solution (10 mL) of $HC(3,5\text{-}Me_2pz)_3$ (0.23 g, 0.76 mmol). Upon addition of the ligand, the desired product precipitated from solution as a pale yellow solid (0.29 g, 92%), dec 340 °C. The crystals used for X-ray crystallographic and magnetic studies were grown by layering a saturated methylene chloride solution with hexanes and allowing the two layers to slowly combine. ^{1}H NMR (CD_2Cl_2): δ 141.8 (2, v br, *H*C), 52.9, −89.6 (18, 18, v br, v br, Me_2), 50.8 (6, v br, 4-*H* pz). Anal. Calcd for $C_{32}H_{44}B_2CoF_8N_{12}$: C, 46.34; H, 5.35. Found: C, 45.91; H, 5.05.

$\{Ni[HC(3,5\text{-}Me_2pz)_3]_2\}(BF_4)_2$ (3). $Ni(BF_4)_2\cdot 6H_2O$ (0.15 g, 0.65 mmol) was suspended in THF (10 mL) and treated dropwise by cannula transfer with a THF solution (10 mL) of $HC(3,5\text{-}Me_2pz)_3$ (0.39 g, 1.3 mmol). Upon addition of the ligand, the desired product precipitated from solution as a pale purple solid (0.35 g, 66%), dec 280 °C. The crystals used for X-ray crystallographic and magnetic studies were grown by layering a saturated methylene chloride solution with hexanes and allowing the two layers to slowly combine. ES$^+$ MS *m*/*z* calcd for $\{Ni[HC(3,5\text{-}Me_2pz)_3]_2\}(BF_4)^+$ 741.3200; found 741.3207.

$\{Cu[HC(3,5\text{-}Me_2pz)_3]_2\}(BF_4)_2$ (4). $Cu(BF_4)_2\cdot xH_2O$ (0.13 g, ca. 0.55 mmol) was suspended in THF (10 mL) and treated dropwise by cannula transfer with a THF solution (10 mL) of $HC(3,5\text{-}Me_2pz)_3$ (0.33 g, 1.1 mmol). Upon addition of the ligand, the desired product precipitated from solution as a pale blue powder (0.37 g, 81%), dec 290 °C. The crystals used for X-ray crystallographic and magnetic studies were grown by layering a saturated methylene chloride solution with hexanes and allowing the two layers to slowly combine. Anal. Calcd for $C_{32}H_{44}B_2CuF_8N_{12}$: C, 46.09; H, 5.32. Found: C, 45.97; H, 5.19.

Crystallographic Studies. 220 K. Crystal, data collection, and refinement parameters are given in Tables 1 and 2. A colorless bar crystal (**2**), a colorless block (**3**), and a blue-green prismatic crystal (**4**) were coated in inert oil, mounted on the end of a thin glass fiber, and transferred to the cold stream of a Bruker SMART APEX

Table 2. Crystallographic Data for the Low Temperature Structures of {Co[HC(3,5-Me$_2$pz)$_3$]$_2$}(BF$_4$)$_2$ (**2**), {Ni[HC(3,5-Me$_2$pz)$_3$]$_2$}(BF$_4$)$_2$ (**3**), and {Cu[HC(3,5-Me$_2$pz)$_3$]$_2$}(BF$_4$)$_2$ (**4**)

	2	**3**	**4**
formula	$CoN_{12}C_{32}H_{44}B_2F_8$	$NiN_{12}C_{32}H_{44}B_2F_8$	$CuN_{12}C_{32}H_{44}B_2F_8$
fw	829.34	829.12	833.95
space group	$P\bar{1}$	$P\bar{1}$	$P\bar{1}$
temp, K	148	125	125
cryst syst	triclinic	triclinic	triclinic
a, Å	10.2702(19)	10.261(4)	10.282(4)
b, Å	11.340(2)	11.327(4)	11.326(4)
C, Å	19.099(4)	18.952(7)	18.788(7)
α, deg	91.159(3)	91.130(9)	90.094(7)
β, deg	104.860(3)	104.627(5)	104.930(6)
γ, deg	116.491(3)	116.302(11)	116.508(12)
V, Å^3	1900.7(6)	1888.4(11)	1874.6(12)
Z	2	2	2
ρ(calcd), g cm^{-3}	1.449	1.458	1.477
μ(Mo Kα), cm^{-1}	5.33	5.96	6.65
R1(*F*)[a], wR2(F^2)[a]	0.0685, 0.1691	0.0897, 0.2051	0.0658, 0.1670

[a] $R1 = \sum||F_o| - |F_c||/\sum|F_o|$. $wR2 = \{\sum[w(F_o^2 - F_c^2)^2]/\sum[w(F_o^2)^2]\}^{1/2}$; $w = 1/[\sigma^2(F_o^2) + (aP)^2 + bP]$, where P is $[2F_c^2 + \max(F_o^2, 0)]/3$.

CCD-based diffractometer system (Mo Kα radiation, $\lambda = 0.71073$ Å).[9] X-ray intensity data were measured at 220(2) K.

Crystal quality and initial unit cell parameters were determined on the basis of reflections taken from a set of three scans measured in orthogonal regions of reciprocal space. Subsequently, a sphere of frame data was collected with a scan width of 0.3° in *ω* and an exposure time of 20 s (**2**), 30 s (**3**), and 10 s (**4**) per frame. The first 50 frames were re-collected at the end of the data set to monitor crystal decay. The raw data frames were integrated into reflection intensity files using SAINT+,[7] which also applied corrections for Lorentz and polarization effects. Analysis of the data showed negligible crystal decay during data collection. No correction for absorption was applied.

Systematic absences in the intensity data for **2**−**4** were consistent with the space group *C*2/*c*. The structures were solved by a combination of direct methods and difference Fourier syntheses and refined by full-matrix least-squares against F^2, using the SHELXTL software package.[8] The Co, Ni, and Cu atoms reside on crystallographic inversion centers; the asymmetric unit consists of the metal atom, one ligand, and one BF_4^- counterion. All non-hydrogen atoms were refined with anisotropic displacement parameters; hydrogen atoms were placed in idealized positions and refined using a riding model.

Low Temperature. Below 165(2) K (**2**) and 155(2) K (**4**), many of the well-shaped diffraction maxima from the C-centered monoclinic form of {M[HC(3,5-Me$_2$pz)$_3$]$_2$}(BF$_4$)$_2$ were observed to split into two peaks, and the data could not be indexed satisfactorily. Upon warming the crystal above 165(2) (**2**), 155(2) K (**4**), the split reflections coalesced, and straightforward indexing of the C-centered monoclinic cell was possible. Cooling the crystal below 165 (**2**), 155 K (**4**), again reproduced the split peaks. The sub-165/155 K form was identified as a nonmerohedral twin with two components. The temperature at which **3** transforms from the C-centered monoclinic form to the low-temperature triclinic form was not well defined but probably occurs near 163 K. On the basis of trials with several different crystals, the number of reflections which fit poorly to the high temperature monoclinic cell gradually increased as it was cooled from room temperature. Near 163 K, a large enough proportion could not be indexed that the crystal was considered twinned. No color change in the crystals accompanied the structural transition. Identification of the twinning, determination of the twin law, and preparation of the reflection files for refinement were carried out using the GEMINI[8] suite of programs.

To acquire enough data for analysis of the twinning, 1800 raw data frames (0.3° width in *ω*, 10 s per frame) (for **3**, 1200 raw data frames were collected and each frame was exposed for 60 s because of the weak scattering power of the small crystal) comprising a full sphere of data in reciprocal space was collected at 148(2) for **2**, and 125(2) K for **3** and **4**.[8] For **2**, a set of 670 reflections randomly thresholded from the data set; the first twin component indexed with 571 reflections ($a = 10.292(2)$ Å, $b = 11.363(2)$ Å, $c = 19.128(3)$ Å, $\alpha = 91.153(3)°$, $\beta = 104.872(3)°$, $\gamma = 116.544(3)°$, $V = 1910.6(5)$ Å^3). Of the remaining 351 reflections, 349 indexed to the second component with similar lattice constants. For **3**, a set of 643 reflections randomly thresholded from the data set; the first twin component indexed with 392 reflections. Of the remaining 251 reflections, 192 were indexed to the second twin component. The 59 remaining reflections fit neither component, and probably belong to a third twin domain. For **4**, a set of 999 reflections randomly thresholded from the data set; the first twin component indexed with 648 reflections ($a = 10.282(4)$ Å, $b = 11.326(4)$ Å, $c = 18.788(7)$ Å, $\alpha = 90.094(7)°$, $\beta = 104.930(6)°$, $\gamma = 116.508(6)°$, $V = 1874.6(12)$ Å^3). Of the remaining 351 reflections, 349 indexed to the second component with similar lattice constants. The two twin components are related by a 180° rotation around the (100) axis in real space. The orientation matrixes (unit cells) for both components were input into SAINT+[7] for integration of the raw frame data. A reflection file for each component was obtained consisting of nonoverlapped reflections and reflections suffering from varying degrees of overlap with the complementary component.

An initial model using only the nonoverlapped data from the major twin component was attempted. Preliminary atomic positions were taken from the published structure of the twinned Fe analogue.[4d] Because of the high degree of overlap between twin components, this model resulted in an unacceptably low data-to-parameter ratio. This result, combined with the relatively equal twin component volumes, necessitated the refinement of all data from both twin components, using the HKLF 5 option in SHELX.[8] The HKLF 5 file was set up as follows: Reflections were sorted on the basis of the degree of overlap into groups, from a separation of 0.000 Å^{-1} in reciprocal space (complete overlap) to 0.035 Å^{-1} (nonoverlapped) and assigned separate batch scale factors (BASF). The increment for the groups was 0.007 Å^{-1} for **2** and 0.005 Å^{-1} for **4**. Reflections separated by greater than 0.035 Å^{-1} were considered nonoverlapped. The refinement used 9 BASF parameters (**2**), 13 BASF parameters (**4**). With this treatment, the refinement proceeded smoothly and converged at R1 = 0.0658 (wR2 = 0.1670) for **2**, R1 = 0.0897 (wR2 = 0.2051) for **3**, and R1 = 0.0685 (wR2 = 0.1691) for **4**. The largest peak and hole remaining in the difference map are 0.92 and 0.74 e$^-$/Å^3, respectively, for **2**, 2.08 and −1.43 and 1.33 e$^-$/Å^3 for **3**, and −0.99 e$^-$/Å^3 for **4**.

For **3**, in all of the crystals screened at 125 K, a nonnegligible set of reflections could not be indexed to either twin domain. Because all sampled crystals were checked at RT to verify quality before cooling, these misfit reflections probably arise from twinning into more than two components during the transformation. The crystal chosen for analysis showed the smallest fraction of reflec-

(7) *SMART Version 5.624*; Bruker Analytical X-ray Systems, Inc.: Madison, WI, 1998. *SAINT+ Version 6.2a*; Bruker Analytical X-ray Systems, Inc.: Madison, WI, 1998.
(8) Sheldrick, G. M. *SHELXTL Version 5.1*; Bruker Analytical X-ray Systems, Inc.: Madison, WI, 1997.
(9) Figgis, B. N. *Introduction to Ligand Fields*; Wiley-Interscience: New York, 1966; p 274.

tions that could not be indexed to either of the two domains. Because the twinning in $\{Ni[HC(3,5\text{-}Me_2pz)_3]_2\}(BF_4)_2$ takes the form of a very slight misalignment of the reciprocal lattices of the two domains, only reflections at higher scattering angle (further from the reciprocal lattice origin of both twins) are completely nonoverlapped. The weak scattering power of the current sample means that fewer high-angle reflections are present. Therefore, the refinement must include a larger proportion of data suffering from partial and compete overlap, whose intensities may not be as accurately determined as nonoverlapped data. These factors, in combination with the presence of a small fraction of a third twin domain, give rise to a poorer data-to-parameter ratio than ideal, relatively high *R*-factors, the need for a global SHELX DELU command for the thermal parameters (164 individual restraints), and the presence of the large residual electron density peaks near the Ni atoms.

Results and Discussion

Syntheses of the Complexes. The reaction of $M(BF_4)_2 \cdot xH_2O$ (M = Co, Ni, and Cu) and $HC(3,5\text{-}Me_2pz)_3$ in a 1:2 ratio yields $\{Co[HC(3,5\text{-}Me_2pz)_3]_2\}(BF_4)_2$ (**2**), $\{Ni[HC(3,5\text{-}Me_2pz)_3]_2\}(BF_4)_2$ (**3**), and $\{Cu[HC(3,5\text{-}Me_2pz)_3]_2\}(BF_4)_2$ (**4**), respectively.

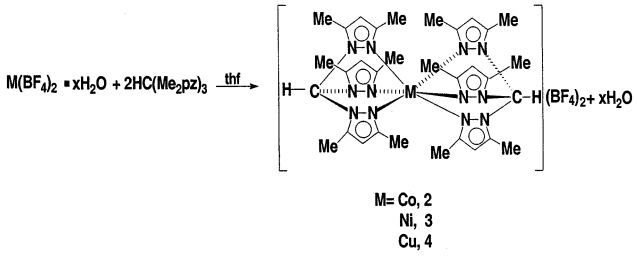

All of these complexes are insoluble in THF and precipitate from the reaction mixture. They are air stable and are soluble in acetone and methylene chloride. The ^1H NMR spectrum of **2** is broad, as expected for a paramagnetic complex, with peaks ranging from −89.6 to 147.8 ppm. ^1H NMR spectra of **3** and **4** could not be obtained because of the line broadening.

Magnetic Studies. All of the complexes studied herein are expected to be dilute paramagnetic complexes that exhibit Curie law behavior with negligible Weiss temperatures and no long-range magnetic exchange interactions, at least above 5 K. Further, the observed phase transitions would be expected to have virtually no influence upon the observed magnetic properties. Indeed, this is found to be the case for microcrystalline samples of **2**−**4**, as is indicated by the Curie constants and the corresponding average effective magnetic moments given in Table 3. For all complexes, the inverse molar magnetic susceptibilities are linear between 5 and 350 K, and the Weiss constants, obtained upon extrapolation to zero temperature, are less than ±1 K.

A plot of the inverse magnetic susceptibility and the effective magnetic moment, μ_{eff}, versus $kT/|\lambda|$ for microcrystalline $\{Co[HC(3,5\text{-}Me_2pz)_3]_2\}(BF_4)_2$, **2**, is shown in Figure 1. In this plot, the $\lambda = -172$ cm^{-1} free ion value of the cobalt(II) spin−orbit coupling constant has been reduced by 15% to −146 cm^{-1}. The observed temperature dependence of the effective moment is totally consistent with that

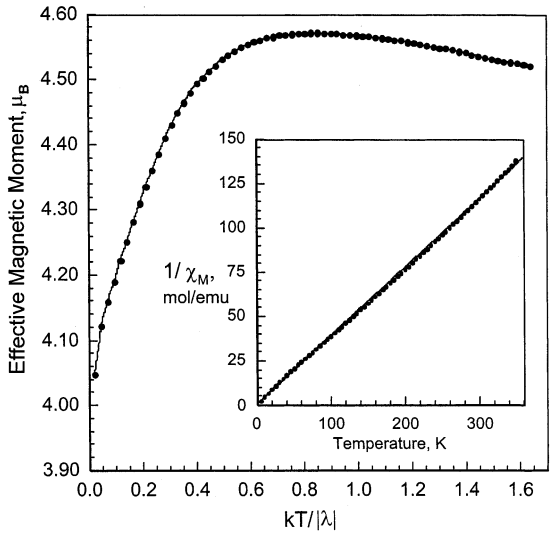

Figure 1. Inverse magnetic susceptibility as a function of temperature (insert) and the effective magetic moment as a function of $kT/|\lambda|$ for microcrystalline $\{Co[HC(3,5\text{-}Me_2pz)_3]_2\}(BF_4)_2$, **2**. In this plot, the $\lambda = -172$ cm^{-1} free ion value of the cobalt(II) spin−orbit coupling constant has been reduced by 15% to −146 cm^{-1}.

Table 3. Magnetic Properties of $\{Co[HC(3,5\text{-}Me_2pz)_3]_2\}(BF_4)_2$ (**2**), $\{Ni[HC(3,5\text{-}Me_2pz)_3]_2\}(BF_4)_2$ (**3**), and $\{Cu[HC(3,5\text{-}Me_2pz)_3]_2\}(BF_4)_2$ (**4**)

	2	**3**	**4**
temp range, K	5−350	5−320	5−345
Curie constant, (mol/emu)/K	2.599	1.294	0.430
av effective magnetic moment, μ_B	4.56	3.22	1.85

expected[9] of cobalt(II) in a distorted octahedral environment with a nominal $^4T_{1g}$ electronic ground state in the presence of spin−orbit coupling. As expected, the results are the same upon heating and cooling, and there is no indication of any significant change at the phase transition.

For both $\{Ni[HC(3,5\text{-}Me_2pz)_3]_2\}(BF_4)_2$, **3**, and $\{Cu[HC(3,5\text{-}Me_2pz)_3]_2\}(BF_4)_2$, **4**, the average effective magnetic moment obtained from the Curie constant, and its temperature dependence, are both consistent with the nominal $^3A_{2g}$ and ^2E_g electronic ground states expected of the nickel(II) and copper(II) ions in a distorted octahedral environment and are indicative of the presence of the expected two and one unpaired electrons, respectively.

All of the described magnetic properties have been obtained on microcrystalline samples of **2**−**4**. In contrast, as we have reported[4] previously for crystalline samples of **1** and observed herein for crystalline samples of **2**−**4**, the magnetic susceptibility obtained upon the initial cooling is nonsuperimposable upon the subsequent warming and cooling susceptibilities because of the crystals physically reorienting in the applied magnetic field at lower temperatures. As has been shown previously[10] for different compounds, this reorientation upon initial cooling is the result of the torque experienced by the crystals because of their expected strong directional magnetic anisotropy. No such reorientation is observed for the microcrystalline samples studied herein.

(10) Sessoli, R.; Tsai, H.-L.; Schake, A. R.; Wang, S.; Vincent, J. B.; Folting, K.; Gatteschi, D.; Christou, G.; Hendrickson, D. N. *J. Am. Chem. Soc.* **1993**, *115*, 1804 and references therein.

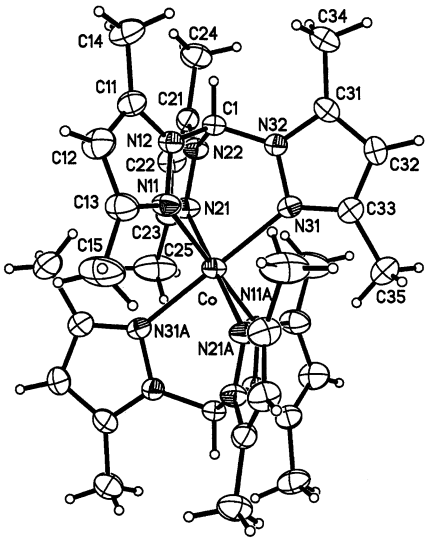

Figure 2. ORTEP diagram of the cation in $\{Co[HC(3,5\text{-}Me_2pz)_3]_2\}(BF_4)_2$ obtained at 220 K.

220 K Solid-State Structures. The solid-state structures for $\{Co[HC(3,5\text{-}Me_2pz)_3]_2\}(BF_4)_2$ (**2**), $\{Ni[HC(3,5\text{-}Me_2pz)_3]_2\}(BF_4)_2$ (**3**), and $\{Cu[HC(3,5\text{-}Me_2pz)_3]_2\}(BF_4)_2$ (**4**) have been determined at 220 K. All of the systems are isomorphous and crystallize in the monoclinic space group *C*2/*c*. An ORTEP diagram of the cation in **2**, representative of the numbering scheme for all three cations, is shown in Figure 2, and Tables 4−6 give selected bond distances and angles. In all cases, the metal is located on a unique crystallographic site which lies on a center of symmetry. For **2**, the average Co−N bond distance is 2.13 Å. The chelate rings restrict the intraligand N−Co−N bond angles to an average of 84.7°, producing a trigonally distorted octahedral structure. The structure of **3** is similar, with an average Ni−N bond distance of 2.09 Å and average N−Ni−N intraligand bond angles of 85.9°. For **4**, the average Cu−N bond distance is similar to that of the cobalt and nickel analogues at 2.13 Å, but because of the Jahn−Teller distortion, two of the Cu−N distances are similar at 2.0229(16) and 2.0668(16) Å, while the third is much larger at 2.3001(17) Å. The chelate rings restrict the intraligand N−Cu−N angles to an average of 85.0°. Even though the Cu−N bond distances are very different, this difference is not reflected in the spread of angles when compared to **2** and **3**.

These three structures are isomorphous to the structure of $\{Fe[HC(3,5\text{-}Me_2pz)_3]_2\}(BF_4)_2$ (**1**) that was also measured at 220 K.[4d] For **1**, the average Fe−N bond distance is 2.17 Å, and the intraligand bond angles average 84.3°.

Low-Temperature Solid-State Structures. The solid-state structures of **2**−**4** were also determined at low temperature (148 K for **2** and 125 K for **3** and **4**). Cooling crystals of **2**−**4** to low temperatures leads to the observation of a phase change. All three systems change from monoclinic to triclinic in the new space group $P\bar{1}$ with nonmerohedral twinning. This change yields two crystallographically unique metal sites. Selected bond distances and angles for the low-temperature structures are given in Tables 4−6. The numbering scheme for one form (labeled low torsion angle form, vide infra) is the same as that shown in Figure 2 while an ORTEP diagram showing the numbering scheme for the other form of the low-temperature structure (labeled high torsion angle form) is shown in Figure 3. The bond angles and distances for the two different metal sites for each compound in the low temperatures structures are very similar to each other and to those in the 220 K structures. For

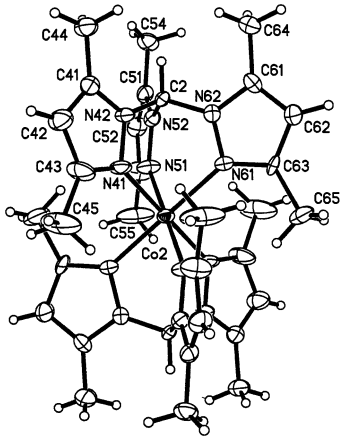

Figure 3. ORTEP diagram of the cation in $\{Co[HC(3,5\text{-}Me_2pz)_3]_2\}(BF_4)_2$ obtained at 125 K (high torsion angle form).

Table 4. Selected Bond Distances and Angles for $\{Co[HC(3,5\text{-}Me_2pz)_3]_2\}(BF_4)_2$ for Data Collected at 220 K and at 148 K

Bond Distances (Å)

	220	148 low torsion angle form	148 high torsion angle form
Co(1, 2)−N(11, 41)	2.1326(19)	2.137(7)	2.116(6)
Co(1, 2)−N(21, 51)	2.1143(19)	2.124(6)	2.124(6)
Co(1, 2)−N(31, 61)	2.1390(19)	2.156(6)	2.136(6)
C(1, 2)−N(12, 42)	1.443(3)	1.448(9)	1.464(9)
C(1, 2)−N(22, 52)	1.437(3)	1.448(9)	1.444(9)
C(1, 2)−N(32, 62)	1.449(3)	1.436(8)	1.432(8)
N(11, 41)−N(12, 42)	1.372(2)	1.385(8)	1.391(8)
N(21, 51)−N(22, 52)	1.370(2)	1.374(8)	1.370(8)
N(31, 61)−N(32, 62)	1.372(2)	1.364(8)	1.355(8)
distance Co out of N_3 donor plane	1.339	1.3356	1.3412

Bond and Torsion Angles (deg)

	220	148 low torsion angle form	148 high torsion angle form
N(11, 41)−Co(1, 2)−N(21, 51)	84.07(8)	86.3(2)	85.2(2)
N(11, 41)−Co(1, 2)−N(31, 61)	84.84(8)	85.3(2)	84.0(2)
N(21, 51)−Co(1, 2)−N(31, 61)	85.05(8)	83.7(2)	83.9(3)
N(11, 41)−Co(1, 2)−N(21A, 51A)	95.93(8)	93.7(2)	94.8(2)
N(11, 41)−Co(1, 2)−N(31A, 61A)	95.16(8)	94.7(2)	96.0(2)
N(21, 51)−Co(1, 2)−N(31A, 61A)	94.95(8)	96.3(2)	96.1(3)
N(11, 41)−N(12, 42)−C(1, 2)	119.20(18)	119.0(6)	118.9(5)
N(21, 51)−N(22, 52)−C(1, 2)	119.27(18)	119.9(5)	119.2(5)
N(31, 61)−N(32, 62)−C(1, 2)	119.25(18)	115.9(4)	119.6(6)
N(12, 42)−C(1, 2)−N(22, 52)	111.73(18)	111.1(6)	112.3(5)
N(12, 42)−C(1, 2)−N(32, 62)	110.69(18)	111.3(5)	110.0(5)
N(22, 52)−C(1, 2)−N(32, 62)	110.83(18)	111.1(6)	110.6(6)
Co(1, 2)−N(11, 41)−N(12, 42)C(11, 41) torsion angle	172.41(15)	166.0(4)	178.4(3)
Co(1, 2)−N(21, 51)−N(22, 52)C(21, 51) torsion angle	167.28(15)	160.1(4)	174.8(4)
Co(1, 2)−N(31, 61)−N(32, 62)C(31, 61) torsion angle	170.84(16)	168.6(4)	179.4(4)

Table 5. Selected Bond Distances and Angles for $\{Ni[HC(3,5\text{-}Me_2pz)_3]_2\}(BF_4)_2$ for Data Collected at 220 K and at 125 K (Low and High Torsion Angle Form)

Bond Distances (Å)

	220	125 low torsion angle form	125 high torsion angle form
Ni(1, 2)−N(11, 41)	2.096(2)	2.128(7)	2.085(7)
Ni(1, 2)−N(21, 51)	2.076(2)	2.082(7)	2.076(6)
Ni(1, 2)−N(31, 61)	2.088(2)	2.109(7)	2.106(7)
C(1, 2)−N(12, 42)	1.441(3)	1.461(10)	1.437(9)
C(1, 2)−N(22, 52)	1.438(3)	1.452(10)	1.428(10)
C(1, 2)−N(32, 62)	1.446(3)	1.452(10)	1.461(10)
N(11, 41)−N(12, 42)	1.367(3)	1.355(9)	1.366(9)
N(21, 51)−N(22, 52)	1.365(3)	1.385(9)	1.357(9)
N(31, 61)−N(32, 62)	1.370(3)	1.376(9)	1.384(9)
distance Ni out of N_3 donor plane	1.288	1.294	1.292

Bond and Torsion Angles (deg)

	220	125 low torsion angle form	125 high torsion angle form
N(11, 41)−Ni(1, 2)−N(21, 51)	85.30(9)	86.2(3)	85.5(3)
N(11, 41)−Ni(1, 2)−N(31, 61)	86.05(8)	85.3(3)	86.0(3)
N(21, 51)−Ni(1, 2)−N(31, 61)	86.26(9)	87.0(3)	85.9(3)
N(11, 41)−Ni(1, 2)−N(21A, 51A)	94.70(9)	93.8(3)	94.5(3)
N(11, 41)−Ni(1, 2)−N(31A, 61A)	93.95(8)	94.7(3)	94.0(3)
N(21, 51)−Ni(1, 2)−N(31A, 61A)	93.74(9)	93.0(3)	94.1(3)
N(11, 41)−N(12, 42)−C(1, 2)	118.9(2)	119.0(7)	121.0(7)
N(21, 51)−N(22, 52)−C(1, 2)	119.0(2)	119.5(6)	118.3(5)
N(31, 61)−N(32, 62)−C(1, 2)	118.6(2)	121.07(7)	116.0(5)
N(12, 51)−C(1, 2)−N(22, 52)	111.7(2)	111.0(7)	111.0(7)
N(12, 42)−C(1, 2)−N(32, 62)	110.8(2)	110.3(6)	110.2(6)
N(22, 52)−C(1, 2)−N(32, 62)	110.6(2)	109.8(7)	111.2(7)
Ni(1, 2)−N(11, 41)−N(12, 42)C(11, 41) torsion angle	173.87(17)	169.0(6)	179.6(5)
Ni(1, 2)−N(21, 51)−N(22, 52)C(21, 51) torsion angle	168.69(17)	161.2(5)	177.4(5)
Ni(1, 2)−N(31, 61)−N(32, 62)C(31, 61) torsion angle	172.30(18)	166.1(5)	179.1(5)

Table 6. Selected Bond Distances and Angles for $\{Cu[HC(3,5\text{-}Me_2pz)_3]_2\}(BF_4)_2$ for Data Collected at 220 K and at 125 K (Low and High Torsion Angle Form)

Bond Distances (Å)

	220	125 low torsion angle form	125 high torsion angle form
Cu(1, 2)−N(11, 41)	2.0668(16)	2.046(3)	2.046(3)
Cu(1, 2)−N(21, 51)	2.0229(16)	2.026(2)	2.029(2)
Cu(1, 2)−N(31, 61)	2.3001(17)	2.349(2)	2.308(3)
C(1, 2)−N(12, 42)	1.444(2)	1.453(3)	1.448(3)
C(1, 2)−N(22, 52)	1.439(2)	1.439(4)	1.447(4)
C(1, 2)−N(32, 62)	1.450(2)	1.434(4)	1.445(4)
N(11, 41)−N(12, 42)	1.372(2)	1.373(3)	1.367(4)
N(21, 51)−N(22, 52)	1.3714(19)	1.383(4)	1.358(4)
N(31, 61)−N(32, 62)	1.367(2)	1.374(3)	1.362(4)
distance Cu out of N_3 donor plane	1.326	1.326	1.326

Bond and Torsion Angles (deg)

	220	125 low torsion angle form	125 high torsion angle form
N(11, 41)−Cu(1, 2)−N(21, 51)	85.26(6)	85.90(10)	85.32(11)
N(11, 41)−Cu(1, 2)−N(31, 61)	85.30(7)	85.56(10)	84.11(11)
N(21, 51)−Cu(1, 2)−N(31, 61)	84.36(6)	83.87(9)	85.16(10)
N(11, 41)−Cu(1, 2)−N(21A, 51A)	94.74(6)	94.10(10)	94.68(11)
N(11, 41)−Cu(1, 2)−N(31A, 61A)	94.70(7)	94.44(10)	95.89(11)
N(21, 51)−Cu(1, 2)−N(31A, 61A)	95.64(6)	96.16(9)	94.84(10)
N(11, 41)−N(12, 42)−C(1, 2)	119.67(14)	119.4(2)	120.4(3)
N(21, 51)−N(22, 52)−C(1, 2)	117.65(11)	119.9(2)	120.2(2)
N(31, 61)−N(32, 62)−C(1, 2)	118.41(14)	118.2(2)	118.8(2)
N(12, 51)−C(1, 2)−N(22, 52)	110.98(14)	110.2(2)	111.0(3)
N(12, 42)−C(1, 2)−N(32, 62)	111.37(14)	111.8(2)	111.1(2)
N(22, 52)−C(1, 2)−N(32, 62)	110.84(14)	111.4(2)	110.8(2)
Cu(1, 2)−N(11, 41)−N(12, 42)C(11, 41) torsion angle	170.22(13)	165.4(2)	177.4(2)
Cu(1, 2)−N(21, 51)−N(22, 52)C(21, 51) torsion angle	168.09(12)	161.63(19)	179.48(18)
Cu(1, 2)−N(31, 61)−N(32, 62)C(31, 61) torsion angle	167.73(13)	158.40(18)	171.88(19)

example, with **2**, the average Co−N bond distances are within 0.01 Å of each other.

We have previously reported that a similar phase change is observed with **1** and all four low-temperature structures are isomorphous. In contrast to the results reported for **2**−**4**, with **1** there is a drastic change in the low-temperature structure when compared to the 220 K structure. In **1**, half of the cations greatly reduce their average Fe−N distance to 1.98 Å because of the change to LS iron(II), whereas the other half (the low temperature HS cations) remain essentially constant with the 220 K structure (same average at 2.17 Å).

We have noted previously that with **1** the difference in bond distance between the HS and LS structures is correlated with the degree of tilting the pyrazolyl rings make away from an ideal C_{3v} type arrangement. In the absence of tilting, the MN(n1)−N(n2)C(n1) torsion angles, where n denotes the ring number, would be 180°, and the metal atom would reside in the planes defined by the pyrazolyl rings. We have shown previously that this torsion angle decreases as the size of the metal increases because the bite size of these ligands is largely fixed and increasing the tilting is an important way to accommodate larger metal ions.[11] In the 220 K structure, with the unique HS iron(II) site, this torsion angle averages 168°. In the low-temperature structure after the phase transition, this torsion angle for the LS form has increased to an average of 179° (high torsion angle form). This increase is expected because of the 0.19 Å decrease in Fe−N bond distance caused by the change in spin state from HS to LS. Importantly, in this low-temperature structure, the HS form torsion angle has actually *decreased* when compared to the high-temperature structure to an average of 162° (low torsion angle form), even though there is no change in the Fe−N average bond distance. The difference in the tilting for the two low temperature forms is best seen in Figure 4 where the cations are pictured down the pseudo-3-fold axis. The greater tilting of the pyrazolyl rings in the HS form, the form with the longer Fe−N bond distances, is clearly observable.

As outlined previously, in the low-temperature structures of **2**−**4**, the two nonequivalent sites have remarkably similar bond distances and angles to each other and to those in the 220 K structures. Similar bond distances and angles are expected, in contrast to **1**, because there is no change in the

(11) Reger, D. L.; Wright, T. D.; Little, C. A.; Lamba, J. J. S.; Smith, M. D. *Inorg. Chem.* **2001**, *40*, 3810.

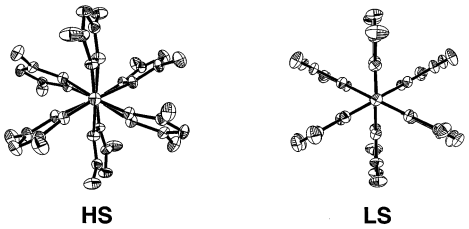

Figure 4. View down the pseudo-3-fold axis of the cation in the high spin (HS) and low spin (LS) forms of {Fe[HC(3,5-Me$_2$pz)$_3$]$_2$}(BF$_4$)$_2$ at low temperature.

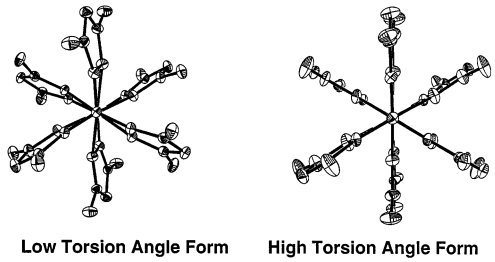

Figure 5. View down the pseudo-3-fold axis of the cation in the low torsion angle form and the high torsion angle form of {Cu[HC(3,5-Me$_2$pz)$_3$]$_2$}(BF$_4$)$_2$ at 125 K.

spin state of either form. Despite this similarity in bond distances and angles, there are major differences *in the MN(n1)−N(n2)C(n1) torsion angles* of the two nonequivalent metal sites in the low-temperature structures, very similar to those observed in iron(II) complex **1**. The view down the pseudo-3-fold axis of symmetry for {Cu[HC(3,5-Me$_2$pz)$_3$]$_2$}(BF$_4$)$_2$ (**4**), which is representative of all three structures, is shown in Figure 5. Although the average Cu−N bond distances for the two forms are the same, in one form, the low torsion angle form, the torsion angle averages 162° whereas in the other form, the high torsion angle form, it averages 176°. As with **1**, the angle in the low torsion angle form is less than the angle found in the 220 structure (169°). Because of the Jahn−Teller distortion, the range of torsion angles in **4** is broader, with a greater tilting observed with the pyrazolyl rings that have the long Cu−N bond distances. The important point is that these changes and differences in torsion angles in the low temperature forms of **2**−**4** are very similar to that observed for **1**, but *come with no significant changes in the M−N bond distances, whereas for **1** the Fe−N bond distances change by 0.19 Å.*

Conclusion

In previous studies of {Fe[HC(3,5-Me$_2$pz)$_3$]$_2$}(BF$_4$)$_2$, it has been shown that in the solid-state the complex is completely HS at 220 K, but below 200 K, the compound undergoes a phase change. This phase change results in half of the cations changing over from the HS state to the LS state, while the other half of the cations remain HS. This change is reversible and takes place in a very organized manner, such that the low-temperature structure contains a 50:50 mixture of HS and LS forms, with the LS form decreasing its Fe−N bond distances by 0.19 Å. The selectivity of this changeover is quite remarkable and could not be fully explained until it was discovered that *this same phase change* is also observed in the solid-state structures reported here for {Co[HC(3,5-Me$_2$pz)$_3$]$_2$}(BF$_4$)$_2$, {Ni[HC(3,5-Me$_2$pz)$_3$]$_2$}(BF$_4$)$_2$, and {Cu[HC(3,5-Me$_2$pz)$_3$]$_2$}(BF$_4$)$_2$. All four compounds are isomorphous at ambient temperatures: monoclinic in the space group *C*2/*c* with *a unique metal site*. Upon cooling, all four undergo the same phase transition and are again isomorphous, changing from monoclinic to triclinic in the new space group $P\bar{1}$ with nonmerohedral twinning. In this system, there are *two different metal sites*. This phase transition is reversible.

The most interesting feature of the changes in structure for all four compounds upon going to low temperature is the changes in the MN(*n*1)−N(*n*2)C(*n*1) torsion angles. In the high-temperature structures, the torsion angles are similar in all four structures and average 168°. Once the phase change has taken place, the torsion angles of one form (corresponding to the HS site for **1**) decrease, while the torsion angles in the second form increase to almost the ideal value of 180° (corresponding to the LS site for **1**). A remarkable feature of this change in torsion angles is that while the bond distances are changing significantly in iron complex **1** (by 0.19 Å), *the change in torsion angles for complexes **2**−**4** comes with no significant change in the bond distances of either form.*

It is now clear that it is the phase transition, which occurs in complexes of the type {M[HC(3,5-Me$_2$pz)$_3$]$_2$}(BF$_4$)$_2$ with first row transition metals, that is driving the unusual spin-crossover behavior of {Fe[HC(3,5-Me$_2$pz)$_3$]$_2$}(BF$_4$)$_2$. Although only one unique metal(II) site is observed above 220 K in all four structures, two sites are observed below the phase transition temperature in all four. In all four cases, one of the two nonequivalent cations has a torsion angle that is at least 10° lower than the other, with the lower angle form actually having *a value lower* than that observed in the high temperature structures. For iron(II), the phase change is accompanied by a spin-state changeover to LS only in the site that shows the increase in torsion angles, a site which has the shorter Fe−N bond distances that favor the higher torsion angles. The other site remains HS and has torsion angles lower than in the all HS high temperature form. The same phase changes are observed for {Co[HC(3,5-Me$_2$pz)$_3$]$_2$}(BF$_4$)$_2$, {Ni[HC(3,5-Me$_2$pz)$_3$]$_2$}(BF$_4$)$_2$, and {Cu[HC(3,5-Me$_2$pz)$_3$]$_2$}(BF$_4$)$_2$, but there are no changes in bond distances. A surprising result is that these changes in torsion angles do not cause half of the cobalt cations to change to the LS form at low temperatures.

The unique result with {Fe[HC(3,5-Me$_2$pz)$_3$]$_2$}(BF$_4$)$_2$ is not that half of the cations change to LS at low temperatures, but that *half do not change*. Many FeN$_6$ complexes are known to change completely over to LS at low temperatures and in some cases show a two-step spin conversion.[1] X-ray crystallography has shown that these changes can be accompanied[12] or not accompanied[13] by a phase change, depending on the system. Interestingly, in most of the cases studied carefully, the metal centers are linked by bridging ligands or hydrogen bonding forces. For compound **1**, the

(12) (a) Garcia, Y.; Kahn, O.; Rabardel, L.; Chansou, B.; Salmon, L.; Tuchagues, J. P. *Inorg. Chem.* **1999**, *38*, 4663. (b) Boinnard, D.; Bousseksou, A.; Dworkin, A.; Savariault, J.-M.; Varret, F.; Tuchagues, J.-P. *Inorg. Chem.* **1994**, *33*, 271.

cations are largely isolated, linked at most by only very weak C−H···F hydrogen bonds. We propose that the phase change, that forces half of the cations to actually decrease the torsion angles in compounds **1**−**4**, energetically *prevents half of the iron(II) centers in **1** from changing over to the LS form* at low temperatures. The increase in the torsion angles forced by the phase change on the other half of the iron(II) centers energetically *favors* the change to LS, explaining the abrupt change in the magnetic moment with temperature.

As an explanation for why the phase change favors half the cations changing to the low torsion angle form, we have calculated the void volume in the unit cells[14] of the low-temperature structures when each of the two types of cations are removed, and those values are shown in Table 7 along with the percent change. As shown in the table, the low torsion angle form occupies a larger volume for complexes **2**−**4** even though the M−N bond distances are the same in both forms. The cations with the more tilted rings take up more space. As expected, the percent difference is largest for **1**, where the bond distances are shorter in the LS form.

Table 7. Void Volume (Å^3) in the Unit Cells upon Removal of the Cation in the Low Temperature Structures of $\{Fe[HC(3,5\text{-}Me_2pz)_3]_2\}(BF_4)_2$ (**1**), $\{Co[HC(3,5\text{-}Me_2pz)_3]_2\}(BF_4)_2$ (**2**), $\{Ni[HC(3,5\text{-}Me_2pz)_3]_2\}(BF_4)_2$ (**3**), and $\{Cu[HC(3,5\text{-}Me_2pz)_3]_2\}(BF_4)_2$ (**4**)

	1	**2**	**3**	**4**
low torsion angle	867	868	856	847
high torsion angle	836	850	836	836
% difference	3.7	2.1	2.4	1.3

The low-temperature crystalline form of these four compounds must be most stable with one smaller and one larger cation, thus *forcing the lower torsion angle arrangement on half of the iron(II) centers in **1** making it energetically more favorable for them to remain HS.*

Acknowledgment. The authors thank the National Science Foundation (CHE-0110493) and the Petroleum Research Fund (36368-AC3) for support. The Bruker CCD single crystal diffractometer was purchased using funds provided by the NSF Instrumentation for Materials Research Program through Grant DMR:9975623. We thank Professors E. Sinn and F. Grandjean and Dr. Paul D. Ellis for helpful discussions on the crystal reorientation observed in the magnetic studies and referees for useful comments.

Supporting Information Available: X-ray crystallographic file, in CIF format, is available. This material is available free of charge via the Internet at http://pubs.acs.org.

IC0112645

(13) (a) van Koningsbruggen, P. J.; Garcia, Y.; Kahn, O.; Fournes, L.; Kooijmam, H.; Spek, A. L.; Haasnoot, J. G.; Moscovici, J.; Provost, K.; Michalowicz, A.; Renz, F.; Gütlich, P. *Inorg. Chem.* **2000**, *39*, 1891. (b) Wiehl, L.; Kiel, G.; Kohler, C. P.; Spiering, H.; Gutlick, P. *Inorg. Chem.* **1986**, *25*, 1565. (c) Garcia, Y.; Guionneau, P.; Bravic, G.; Chasseua, D.; Howard, J. A. K.; Kahn, O.; Ksenofontov, V.; Reiman, S.; Gütlick, P. *Eur. J. Inorg. Chem.* **2000**, 1531.

(14) Spek, A. L. *PLATON, A Multipurpose Crystallographic Tool*; Utrecht University: Utrecht, The Netherlands, 1998.